Plasmonic organic thin-film solar cell: light trapping by using conformal vs. non-conformal relief gratings

Hamid Keshmiri and Jakub Dostalek*
Austrian Institute of Technology GmbH, Muthgasse 11, Vienna 1190, Austria

ABSTRACT

Theoretical study of light management in thin film organic photovoltaic cell that utilizes diffraction coupling to guided waves is presented. As a model system, a regular solar cell geometry with P3HT:PCBM active layer, transparent ITO electrode and Al backside electrode is used. The paper discusses enhancement of absorption of incident photons selectively in the active layer by the interplay of surface plasmon polariton and optical waveguide waves, the effect on the profile of their field and damping that affects the spatial distribution of dissipated light energy in the layer structure. The model shows that for optimized grating period and modulation depth the number of absorbed photons in the active layer can be increased by 24 per cent. The comparison of the geometry with conformal and non-conformally corrugated layers reveals that the conformal structure outperforms the non-conformal in the enhancing of photon absorption in the wavelength range of 350-800 nm.

Keywords: organic solar cell, surface plasmon, light harvesting, numerical calculation

1. INTRODUCTION

We witnessed increasing interest in organic polymer-based photovoltaics (OPV) over the last years [1-2]. In order to enhance the power conversion efficiency (PCE) of OPV cells that is limited by the weak absorption probability in inherently thin absorber layers, light harvesting schemes including those relying on plasmonics were proposed [3]. On breaking the efficiency barrier in 30-100 nm thickness range of the active layer, improving of omnidirectional absorption and photocurrent density have been are pursued by using randomly distributed metallic nanoparticles inside and outside the active layer, and high-order periodic metal arrays incorporated with electrodes [4]. To date, the successful integration of tandem cells along with single-junction principles in polymeric OPVs leads by 9.2%-10.1% PCE [5-6].

The (probably) most thoroughly investigated thin OPV cell utilizes bulk hetero-junction active layer composed of P3HT (poly (3-hexyl-thiophene)):PCBM (phenyl-C61-butyric acid methyl ester) [7]. Such absorber is typically implemented to a solar cell by using a stack of layers including aluminum metallic electrode, LiF, P3HT:PCBM, PEDOT (poly (3, 4-ethy -lenedioxythio-phene)):PSS (poly (styrenesulfonate)), and transparent ITO electrode. This theoretical paper presents a numerical study on the light harvesting in P3HT:PCBM by using a periodically corrugated metallic electrode. The aim is to tune the diffraction grating design to enhance the absorption in the active layer by an interplay of surface plasmon polaritons (SPPs) travelling at the Al electrode and other dielectric waveguide modes supported by the investigated layer structure. General rules for maximizing the dissipation in the absorber and suppressing the competing absorption in other layers are presented based on the knowledge of profile of the field and dispersion of involved guided waves. The presented data illustrate the control of the resonant coupling to guided waves over the visible and near infrared part of solar spectrum.

2. INVESTIGATED GEOMETRY

In the performed study, there was assumed a thin film OPV cell structure depicted in Figure 1 which consists of three layers sandwiched between semi-infinite BK7 glass and Al. The structure was periodically corrugated by a grating that allows for diffraction coupling of far field radiation to guided modes confined in the structure. In the non-conformal geometry, only the Al interface was modulated and other interfaces were flat. In the conformal geometry, all interfaces were identically modulated. Cartesian coordinates were used as showed in the Figure 1. The structure was periodic in y direction and stack of layers was placed in the x direction. All layers were assumed to be infinite in z direction.

Metamaterials X, edited by Vladimír Kuzmiak, Peter Markos, Tomasz Szoplik, Proc. of SPIE
Vol. 9502, 950210 · © 2015 SPIE · CCC code: 0277-786X/15/$18 · doi: 10.1117/12.2180950

Sinusoidal corrugation of the interfaces with the amplitude of a and period Λ was assumed. As an active layer, P3HT:PCBM layer with a thickness of d_a=100 nm was placed on the top of an optically thick Al surface. 50 nm thick PEDOT:PSS with a 150 nm thick transparent electrode of ITO was used above the active layer. The structure was illuminated by a plane-wave propagating from BK7 superstrate under an angle of incidence θ at wavelengths between 350 nm and 850 nm. The real and imaginary parts of refractive index ($\tilde{n} = n + i\kappa$) of P3HT:PCBM were provided through the courtesy of G. Jakopic from Joanneum Research FmbH, Austria. The refractive index of Al was taken from Palik's database [8], ITO's from Sopra database [SOPRA S.A., France], and PEDOT:PSS from [9].

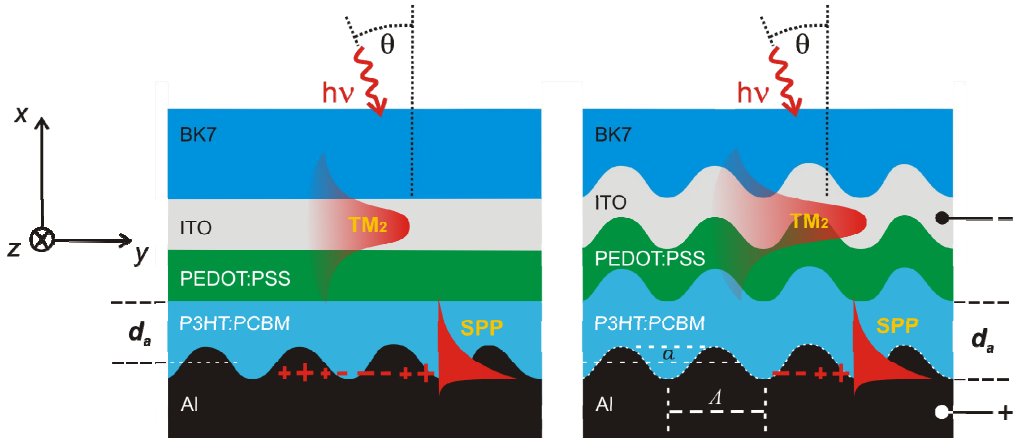

Figure 1. Investigated regular geometry of the OPV cell composed of a metallic cathode, P3HT:PCBM active layer, hole conductive PEDOT:PSS, ITO anode, and BK7 superstrate. The left figure shows the non-conformal structure while the right figure the OPV cell with conformal layer geometry.

3. METHODS

Two-dimensional (2D) electromagnetic simulations based on the finite-difference time-domain method (FDTD) were carried out. The method was implemented in a software tool Lumerical FDTD Solutions (Lumerical Solutions Inc., Canada). A unit cell with the width equal to the period Λ was defined and periodic boundary conditions in x axis were used. In the x direction, perfect matched layer (PML) was placed and a metal boundary condition was applied at the distances of 1 μm and 0.7 μm above and below the layer stack, respectively. A reflectivity monitor was placed behind the source in order to calculate the reflectance of the structure. For simulating the near field distribution through the layer structure, there was employed a line monitor oriented along the x axis. A group of monitors consisting of the refractive index and power monitors were also used in the x-y plane in order to gather data that were further post processed by using script code which calculates the absorbed power in each layer. The simulation of spectrum of modes supported by the investigated structure was calculated by using a model CAMFR [10] that relies on the eigenmode expansion. PMLs were placed at the distance of 1 μm above and below the stack of flat layers and the propagation constant β and profile of field were obtained for selected modes. The efficiency of plasmonic light harvesting was quantified by absorption probability η which was defined as:

$$\eta_i(\lambda) = \frac{1}{P_{inc}} \int_i |E(x,y,\lambda)|^2 \, \mathrm{Re}\{\tilde{n}(\lambda)\} \mathrm{Im}\{\tilde{n}(\lambda)\} \mathrm{dV}\,, \tag{1}$$

where λ is a wavelength, P_{in} is the power of incident plane wave and $|\boldsymbol{E}|^2$ is the electric field intensity generated inside the OPV cell by the incident plane wave. The integration was performed for each layer indexed by i. The simulations were performed at the wavelength range λ=350-800 nm (typically used glass substrates strongly absorb at wavelength λ<350 nm and the absorption of P3HT:PCBM rapidly drops at wavelengths λ>650 - difference in HOMO and LUMO energies is of 770 nm for P3HT and 527 nm for PCBM [7]). The absorption probability in the active layer η_A was integrated over this wavelength range as:

$$\eta_{OA} = \int_{\lambda_1}^{\lambda_2} \eta_A(\lambda)\Phi(\lambda)d\lambda \Big/ \int_0^{\infty} \Phi(\lambda)d\lambda, \quad (2)$$

where λ_1=350 nm and λ_2=800 nm and Φ is the photon flux density of AM1.5 solar spectrum. For simplicity, only 2D geometry and transverse magnetically (TM) polarized light wave that was normally incident at the OPV cell at θ=0 was assumed. It should be noted that the orthogonal transverse electrically (TE) polarized waves can be coupled to discussed modes by used crossed gratings and the simulations can be straightforward extended to a full 3D model.

4. RESULTS AND DISCUSSION

Firstly, let us discuss the spectrum of guided modes that are supported by the investigated structure with parameters that lie in the range used in the majority of reported studies [11]. In the TM polarization, SPPs can be generated at the interface between the Al and P3HT:PCBM active layer in the whole wavelength range λ_1-λ_2. As seen in the profile of field intensity in Figure 2a, the SPP field is mostly confined in the active layer. The penetration depth of SPP field into the OPV cell (defined as the distance $L_p/2$ from Al where the field intensity drops by 1/e) is increasing with the wavelength from $L_p/2$=36 nm at λ=358 nm to $L_p/2$=96 nm at λ=730 nm. Moreover, the high refractive index ITO layer supports additional guided waves that are noted as TM_1 (at wavelength λ<650 nm) and TM_2 (at wavelength λ<400 nm) waves. As illustrated in Figure 2b, the field intensity of TM_1 is mostly concentrated in the ITO layer and only weakly overlaps with the active layer. The TM_2 mode exhibits a minimum inside the ITO and thus its field stretches further into active layer region. In order to couple an incident light wave to SPP and $TM_{1,2}$ modes, diffraction on periodically corrugated surface can be employed. The grating momentum $2\pi/\Lambda$ allows for the phase matching of incident light wave with the guided waves and thus to efficiently transfer energy from the far field to the near field waves travelling along the OPV cell layers:

$$\pm \mathrm{Re}\{\beta\} = \frac{2\pi}{\lambda} n_{sup} \sin(\theta) + m\frac{2\pi}{\Lambda}, \quad (3)$$

where β is the (complex) propagation constant of a guided wave and n_{sup} is the refractive index of the glass superstrate. Figure 2c compares wavelength-dependent dispersion of SPP, TM_1 and TM_2 modes supported by the investigated structure. For the normally incident plane wave (θ=0), these modes can be excited by first order diffraction (m=±1) on a corrugation with the period in the range of Λ=200-400 nm. The phase matching condition (3) is fulfilled at wavelengths, where the grating momentum (represented as a dashed line) crosses a dispersion relation. For the selected periods Λ=200, 300, and 400 nm, the phase-matching with SPPs is marked as 1b, 4 and 6 and it occurs at wavelengths λ=385, 600 and 730 nm, respectively. Similarly, the coupling to TM_1 mode occurs at wavelengths λ=380, 500 and 620 nm for the selected periods Λ and it is marked as 1a, 3, and 5.

Reflectivity spectra in Figure 2d reveal that the coupling to SPP and TM_1 modes manifests itself as a series of reflectivity dips at wavelengths matching those predicted by equation (3). For the short period Λ=200 nm, the absorption (1-R) is enhanced in the blue part of spectrum owing to the first diffraction order coupling to SPP and TM_1 modes at wavelengths around λ~400 nm (marked as 1). Let us note that these resonances are slightly red shifted compared to those obtained from equation (3) due to the presence of the corrugation which alters the properties of modes (described in Figure 2a-c for a flat geometry). When increasing the period to Λ=300 nm, the SPP (marked 4) and TM_1 (marked 3) resonances shift to wavelengths 575 nm and 509 nm, respectively. In addition, one can see a drop of the reflectivity at the wavelength around λ~450 nm which corresponds to crossing the light line (marked 2) and probably interacting with TM_2 mode which has a cut-off close to this wavelength. For the period Λ=400 nm, SPP and TM_1 resonances due to the first diffraction order coupling occur in the red part of spectrum at wavelength λ=610 and 730 nm, respectively. Interestingly for the selected modulation depth the second order diffraction coupling to modes at around 400 nm (similar to that observed for Λ=200 nm) is not apparent.

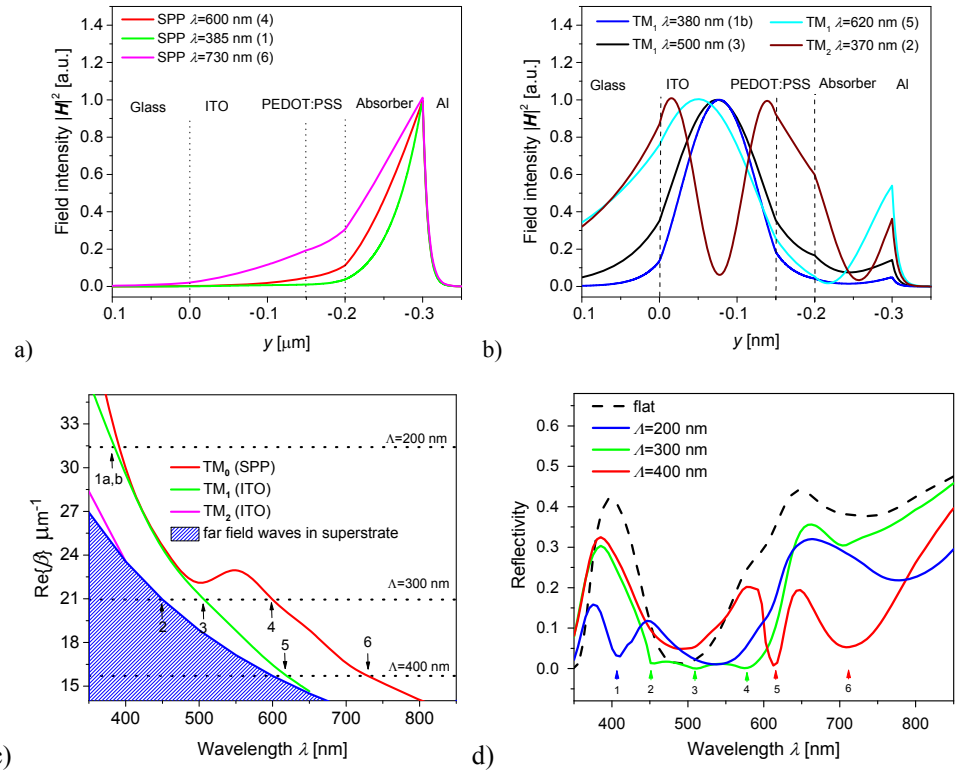

Figure 2. Examples of magnetic field intensity profile $|\boldsymbol{H}|^2$ of a) SPP and b) TM_1 modes across the layer structure and c) respective dispersion relation of supported guided waves in the wavelength range λ=350-850 nm. d) Reflectivity spectrum for a flat OPV cell structure compared to three (non-conformal) corrugated structure OPV cells with the period Λ=200, 300 and 400 nm and modulation amplitude a=30 nm.

As showed by Figure 2a, the diffraction coupling to guided waves substantially broadens the absorption band in the reflectivity spectrum that is associated with the dissipation in the P3HT:PCBM (centered at around λ~500 nm). In particular, the tuning of the corrugation period Λ allows to enhance the dissipation in the OPV layer stack at the shoulders of the P3HT:PCBM absorption band at blue wavelength range (λ<450) and red part of spectrum (λ>550).

In the further section, let us discuss the spatial distribution of the absorption in order to identify optimum geometry that maximizes the dissipation in the P3HT:PCBM absorber and minimizes competing dissipation in other layers. This study was carried out by simulating the spatial distribution of the electric field intensity $|\boldsymbol{E}|^2$ inside the OPV structure as depicted in Figure 3. It shows a cross-section of $|\boldsymbol{E}(-400<x<500,\ y=0)|^2$ for the studied range of wavelengths. Figure 3a reveals that for a reference flat geometry the reflectivity is decreased around the wavelength of 500 nm as can be seen from weaker fringes that originated from the interference of incident and reflected beams. The excitation of guided waves by the first order diffraction in the stack of OPV cell manifests itself as an increased field intensity in either the active layer for SPPs (see Figure 2a) or in the ITO for $TM_{1,2}$ modes (see Figure 2b). These features can be seen for SPP in Figure 3b and c at the wavelength around 650 nm and 750 nm, respectively. Let us note that the wavelength where maximum field enhancement occurs does not exactly coincide with the resonant condition defined by equation (3) owing i) effect of the rapidly decreasing absorption of P3HT:PCBM with a wavelength which shifts the maximum $|\boldsymbol{E}|^2$ to longer wavelengths and ii) the reflectivity minimum wavelength is dependent on additional effects including interference between the directly reflected and out-coupled SPP or TM_1 field that are phase-shifted and lead to more complex behavior. In addition, it should be commented on the fact that the magnetic field intensity profile $|\boldsymbol{H}|^2$ in Figure 2 is continuous across the layer interfaces while the spatial distribution of $|\boldsymbol{E}|^2$ in Figure 3 is not. The reason is that the $\boldsymbol{H}$ vector has only component parallel to the layer surfaces (which is continuous) and the $\boldsymbol{E}$ vector has strong component perpendicular to the surface (particularly for SPPs) which is not continuous when passing an interface between different materials.

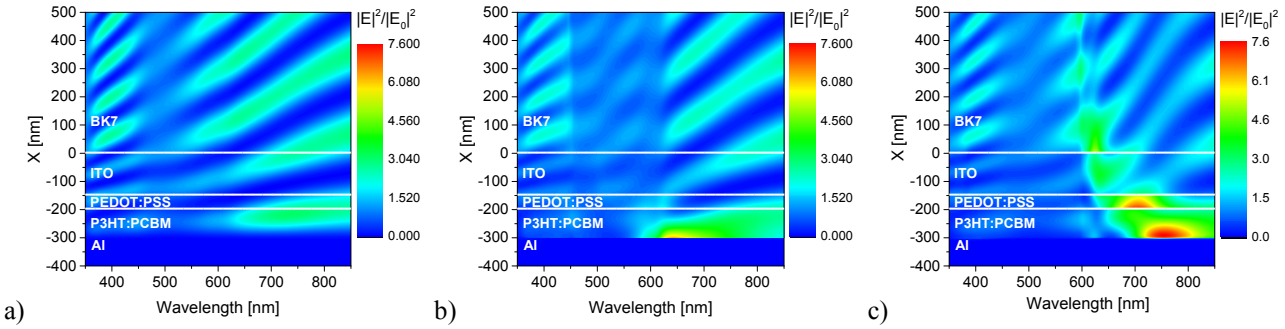

Figure 3. Spatial distribution of electric field intensity $|E/E_0|^2$ for TM polarized normally incident plane wave and a) flat layer structure, b) non-conformal corrugated structure with Λ=300 nm, and c) non-conformal corrugated structure with Λ=400 nm. The modulation amplitude was a=30 nm in b) and c).

The spatial distribution of near field electric intensity $|\boldsymbol{E}|^2$ was used for the calculating of absorption probability η in each layer by using the equation (1). An example in Figure 4 compares the absorption probabilities for two OPV cell geometries: with the only periodically modulated interface between Al and the active layer [non-conformal geometry in the left figure a)] and with all interfaces identically corrugated [conformal geometry in the right figure b)]. These data were calculated for period set to Λ=320 and the modulation amplitude of a=30 nm. In general, one can see that the peak probability of the absorption in the P3HT:PCBM active layer η_A is of about 0.76 at 500 nm for both flat and structured geometries. The diffraction interaction with guided waves enhances η_A below and above the P3HT:PCBM absorption band. At the wavelength of λ=600 nm, the η_A is increased from η_A=0.42 to 0.58 due to the excitation of SPPs. This effect is accompanied by an absorption in Al associated with an increase of η_A from 0.11 to 0.31. As the SPP field penetrates to the PEDOT:PSS, an additionally enhanced absorption in this layer can be seen. Owing to the dominant SPP-assisted absorption of light at the interface between Al and P3HT:PCBM in the wavelength range 600 – 700 nm, the reflectivity is decreased and absorption in ITO is lowered. Inside the P3HT:PCBM absorption band at λ=550 nm, one can see an slightly increased absorption at ITO film that is associated with the coupling to TM_1 mode and which does not affect significantly the η_A as the mode overlaps with P3HT:PCBM only weakly. Lastly, one can see the increase of below the P3HT:PCBM absorption band at the wavelength around 400 nm. This enhancement is probably due to the partial interaction with TM_2 mode (even this wavelength is above its cut-off). One can see that this effect is much stronger for the conformal structure than for the non-conformal one. The reason is indicated by the enhanced absorption at ITO layer at around 400 nm which is more pronounced for the conformal structure. For this geometry the periodical modulation of ITO interfaces leads to stronger coupling to TM_2 mode. As Figure 2b shows, the profile of TM_2 mode exhibit stronger overlap with these areas as well as with P3HT:PCBM absorber and thus (contrary to TM_1) enable substantially increase the η_A.

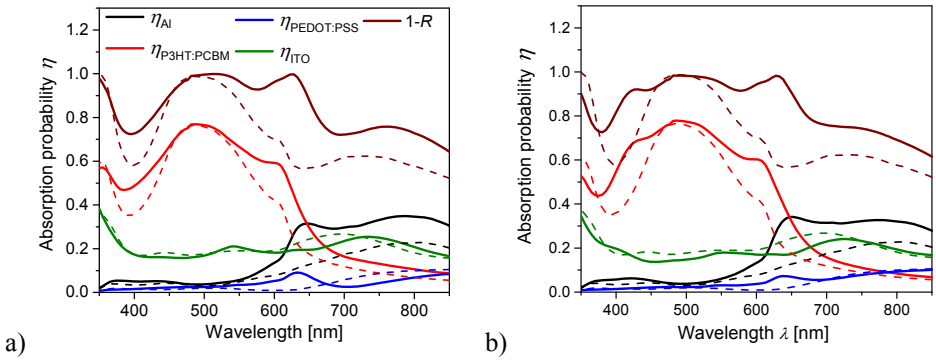

Figure 4. Comparison of the absorption probability in each layer for the solar cells structure with a grating period of Λ=320 nm and the amplitude a=30 nm and a) non-conformal and b) conformal configuration. The dotted line shows for comparison the absorption probabilities for flat layer structure.

Finally, let us investigate how the coupling to the SPP and $TM_{1,2}$ guided modes increases the number of photons absorbed in the P3HT:PCBM active layer. Figure 5a shows the enhancement of the photon absorption which was simulated by using the overall absorption probability η_{OA} defined by equation 2. These data were simulated for periods from Λ=200 to 400 nm and the corrugation amplitude a increasing from 0 to 40 nm. The results reveal that the maximum enhancement occurs for the period of 320 nm and the modulation amplitude around 30 nm. The comparison shows that the conformal structure can outperform the non-conformal and that it allows for 24 per cent increasing the absorption probability of photon flux with AM1.5 spectrum. This value is higher by about 4 per cent that that for the conformal geometry. In general, both geometries benefit from the SPP-enhanced absorption at the higher wavelength region. The reason for the better performance of the conformal structure is its improved absorption in the low wavelength region that is assisted by diffraction-coupled TM_2 mode supported by the ITO layer.

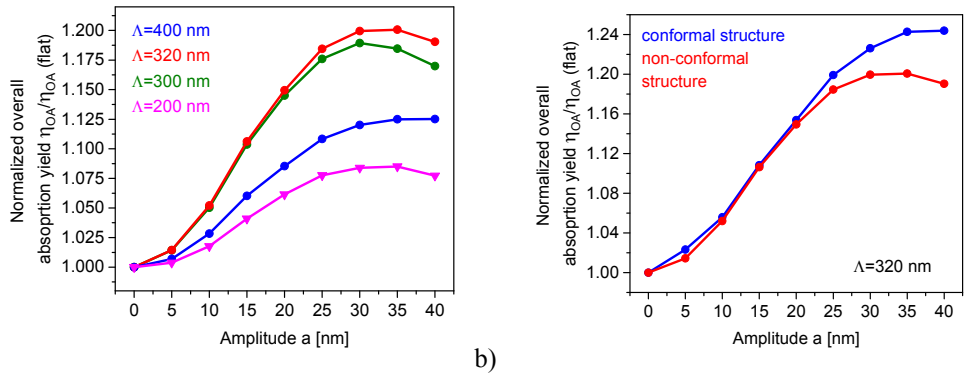

Figure 5. Dependence of the overall absorption probability η_{OA} on the modulation amplitude a for a) non-conformal geometry and periods Λ=200-400 nm and b) comparison between non-conformal and conformal geometry with Λ=320 nm.

CONCLUSION

Thin film organic photovoltaic solar cell with P3HT:PCBM active layer represents a well characterized system that was experimentally utilized and demonstrated the power conversion efficiency of about PCE=2.5 % [7]. In order to enhance the PCE of this and similar thin film OPV cells, the structuring of metallic back electrode was proposed [4]. Depending on the fabrication method, the cells can be prepared as only the metallic surface is structured (e.g. by embossing to the polymer absorber) or when all the layers are corrugated (e.g. by chemical vapor deposition). The presented simulations suggest that the conformal geometry holds potential to increase the amount of photons absorbed at the active layer by 24 per cent which outperforms that with non-conformal geometry for which only 20 per cent enhancement is predicted. In addition, the presented study reveals that the using of SPP modes travelling along the Al surface can offer significant enhancement similar to Au or Ag metals that are more often utilized in plasmonic devices. In addition, the effect of the mode confinement is discussed and identified that the in TM polarization, the using of SPP travelling along the Al surface and TM_2 mode guided by the ITO film is favorable for the light harvesting in the active layer due to the confinement of the field in its region.

ACKNOWLEDGMENT

This research has been supported by the Austrian Institute of Technology GmbH, and the Austrian Science Fund through the project PLASMOSOL - FWF TRP-304-N20.

REFERENCES

[1] Li, G., Zhu, R., Yang, Y., “Polymer solar cells”, Nat. Photonics 6, 153-161 (2012).

[2] Chen, L. M., Hong, Z., Li, G., Yang, Y., “Recent progress in polymer solar cells: manipulation of polymer: fullerene morphology and the formation of efficient inverted polymer solar cells”, Adv. Mater. 21, 1434-1449 (2009).

[3] Atwater, H. A., Polman, A., "Plasmonics for improved photovoltaic devices", Nat. Mater. 9 , 205-213 (2010).
[4] Gan, Q., Bartoli, F. J., Kafafi, Z. H., "Plasmonic-enhanced organic photovoltaics: breaking the 10% efficiency barrier", Adv. Mater. 25, 17, 2385-96 (2013).
[5] Service, R. F., "Outlook brightens for plastic solar cells", Science 332, 293 (2011).
[6] Wu, C., "Thinking small for solar", MRS Bull. 37, 194-195 (2012).
[7] Ludwigs, S., (Ed.), "P3HT Revisited – From Molecular Scale to Solar Cell Devices", Springer-Verlag Berlin Heidelberg (2014).
[8] Palik, E. D., "Handbook of Optical Constants of Solids", Academic Press (1998).
[9] Nam, Y. M., Huh, J., Jo., W. H., "Optimization of thickness and morphology of active layer for high performance of bulk-heterojunction organic solar cells", Sol. Energ. Mat. Sol. Cells 94, 6, 1118-1124 (2010).
[10] Bienstman, P., Baets, R., "Optical modelling of photonic crystals and VCSELs using eigenmode expansion and perfectly matched layers", Opt. Quantum Electron. 33 (4-5), 327-341 (2001).
[11] Li, K., Zhen, H., Huang, Z., Li, G., Liu, X., "Embedded surface relief gratings by a simple method to improve absorption and electrical properties of polymer solar cells", ACS Appl. Mater. Interfaces 4, 8, 4393-4397 (2012).